Applied Catalysis B: Environmental 203 (2017) 116–126

Contents lists available at ScienceDirect

Applied Catalysis B: Environmental

journal homepage: www.elsevier.com/locate/apcatb

Study of $Ag/Ce_xNd_{1-x}O_2$ nanocubes as soot oxidation catalysts for gasoline particulate filters: Balancing catalyst activity and stability by Nd doping

Yuxi Gao[b,1], Anqi Duan[a,1], Shuang Liu[a,*], Xiaodong Wu[b], Wei Liu[a,*], Min Li[c], Shougang Chen[a], Xin Wang[a], Duan Weng[b]

[a] Institute of Materials Science and Engineering, Ocean University of China, Qingdao 266100, China
[b] Key Laboratory of Advanced Materials of Ministry of Education of China, School of Materials Science and Engineering, Tsinghua University, Beijing 100084, China
[c] Haier Group Technique R&D Center, Qingdao 266100, China

ARTICLE INFO

Article history:
Received 18 July 2016
Received in revised form 1 September 2016
Accepted 4 October 2016
Available online 4 October 2016

Keywords:
$Ag/Ce_xNd_{1-x}O_2$ nanocubes
Soot oxidation
Thermal stability
Oxygen vacancies
O_x^- and bulk oxygen

ABSTRACT

Three nanocubic $Ag/Ce_xNd_{1-x}O_2$ catalysts were synthesized to evaluate the influence of Nd doping on catalyst practicability. It was observed that Nd doping generated excessive ceria surface oxygen vacancies, but reduced the bulk oxygen vacancies. These variations in oxygen vacancies suppress the utilization of ceria bulk oxygen, and induce the formation of less active O^{2-} species instead of O_2^-, resulting in a low soot oxidation activity. However, the introduction of Nd can inhibit Ag sintering and thus enhance the catalysts' thermal stability effectively. As a consequence, $Ag/Ce_{0.95}Nd_{0.05}O_2$ nanocubes make a good balance between the catalyst activity and stability. Moreover, it was observed that catalyst deactivation during soot oxidation becomes more obvious when the catalysts and soot are not in close contact.

1. Introduction

Gasoline direct injection (GDI) concepts are the key technology of gasoline engine development to reduce CO_2 emissions while improving torque and power output. However, there is a side effect of increased particle number (PN) emissions of GDI engines compared with conventional Port Fuel Injection engines [1]. One possibility to achieve the proposed Euro 6 legislation PN limit of 6×10^{11} km^{-1} is the introduction of a catalyzed gasoline particulate filter (CGPF) to the exhaust after-treatment system [2]. Based on the vast experience accumulated concerning diesel vehicles, platinum catalysts seem to be the most practical ones for soot oxidation. However, the working condition of GPF is quite different from the diesel particulate filter (DPF), which is because the upstream Three-way Catalyst (TWC) consumes a large content of oxygen and converts most of NO_x into N_2 [3,4]. Based on some earlier studies [5–8], this special working condition may provide opportunities for Ag/CeO_2 versus commercial platinum-based materials as soot oxidation catalysts. Therefore, the application potential of Ag/CeO_2 for CGPF should be explored in detail.

In previous studies [9,10], it was found that monocrystalline nanocubic ceria-based catalysts exhibits a high activity for soot oxidation, and the loading of silver can further improve their catalytic performance [5]. Nevertheless, the practicability of nanocubic Ag/CeO_2 catalysts is questionable since Ag/CeO_2 was reportedly exhibited severe deactivation for soot oxidation after high-temperature ageing [11–13]. Fortunately, Shimizu et al. [13] observed that lanthanum doping can increase the thermal durability of "rice-ball"-like CeO_2-Ag materials, which is in agreement with the well-known knowledge that the introduction of rare-earth metals enhances the stability of ceria [6,14]. As a newly studied rare-earth metal, neodymium has proven itself good additives for ceria-based soot oxidation catalysts [15–17]. Therefore, it is worth trying to evaluate the practicability of Nd-modified nanocubic Ag/CeO_2 catalysts by testing their activity and thermal stability.

Furthermore, based on ceria catalysts with different shapes, we recently evidenced that excessive surface oxygen vacancies ($V_{O\text{-}s}$) may lead to the formation of less active O_x species, which further causes catalyst deactivation during the reaction [5,10]. The universality of this theory should be verified, both on doped ceria catalysts

* Corresponding authors.
E-mail addresses: lius@ouc.edu.cn (S. Liu), weiliu@ouc.edu.cn (W. Liu).
[1] These two authors contributed equally to this work.

http://dx.doi.org/10.1016/j.apcatb.2016.10.006
0926-3373/

and in more practical reaction conditions. As a lanthanide dopant with positive association energies, Nd can increase the conversion rate from Ce^{4+} ionization state to Ce^{3+} state and consequently increase the oxygen vacancies in ceria nanoparticles [18]. In this sense, Ag/CeO_2 doped with Nd can be ideal catalyst models for exploration of the above mechanism. What's more, the influence of high-temperature ageing on the catalyst properties may also provide useful information to improve this theory.

In the present study, three Nd-doped Ag/CeO_2 catalysts with similar cube-like shapes and diverse content of oxygen vacancies were synthesized and studied. By comparing their activity and thermal stability, the influence of Nd-doping on catalyst practicability was analyzed in detail.

2. Experimental

2.1. Materials

CeO_2 and $Ce_xNd_{1-x}O_2$ nanocubes were synthesized via a hydrothermal method [5]. During a typical synthesis, $Ce(NO_3)_3{\cdot}6H_2O$ (4 mmol), NaOH (480 mmol) and $Nd(NO_3)_3{\cdot}6H_2O$ (0, 0.2 or 0.4 mmol) were dissolved in 80 mL of distilled water and stirred for 0.5 h. The obtained mixture was heated in a 100 mL stainless autoclave at 180 °C for 24 h. After filtration, washing and calcinations at 550 °C in static air for 3 h, the nanocubic samples were obtained. The supported Ag (5 wt.%) catalysts were prepared via incipient wetness impregnation of the above samples with $Ag(NO_3)_2$ solutions (Aladdin, 99%), followed by drying at 110 °C overnight and calcination at 500 °C for 3 h. Then the fresh catalysts were obtained and denoted as AgCe-F, $AgCeNd_{0.05}$-F ($Ag/Ce_{0.95}Nd_{0.05}O_2$, Nd:Ce = 1:20) and $AgCeNd_{0.1}$-F ($Ag/Ce_{0.9}Nd_{0.1}O_2$, Nd:Ce = 1:10). These catalysts were further treated at 700 °C in 1% O_2/10% H_2O/N_2 for 48 h to obtain the aged samples (labeled with "-A"). This ageing condition was chosen to simulate the working atmosphere of CGPFs [3–5] and full useful life vehicle aging (120 k miles) [19].

2.2. Activity measurements

As previously reported, Printex–U is a reasonable substitute for GDI soot, since they share similar morphologies and oxidation behavior [1,2]. Therefore, Printex–U from Degussa (diameter 25 nm, surface area 100 m^2/g) was used as the model soot in the present study. For each activity test, 10 mg of soot and 100 mg of catalyst were mixed by a spatula for 2 min to achieve "loose-contact" conditions. To minimize the effect of hot spots, this soot-catalyst mixture was further diluted with 300 mg of silica pellets and then sandwiched by quartz wool which placed in a tubular quartz reactor. A gas mixture of 1% O_2/N_2 (500 mL/min) was fed to simulate the working condition of a CGPF roughly [5,10]. Two types of test conditions were applied in this work:

- Temperature-programmed oxidation (TPO) process at a constant heating rate (5 °C/min) from room temperature (RT) to 600 °C. The results can reflect the catalyst activity roughly.
- Isothermal reactions at 300, 350 and 400 °C for 0.5 h, respectively. The results can reveal the catalytic behavior of the samples in detail.

The concentration of CO_2 and CO in the outlet gas was monitored by an infrared spectrometer (Thermo Nicolet iS10). Each test was repeated two times to ensure the reproducibility of the results.

2.3. Characterizations

X-ray powder diffraction analysis of the products was performed using a Bragg–Brentano-type powder diffractometer (D8 ADVANCE, Bruker, Germany, operated at 40 kV and 30 mA, Cu–Ka radiation, λ = 0.15418 nm).

Sample morphologies were observed through a field emission scanning electron microscope (MERLIN VP Compact, ZEISS, Germany), a transmission electron microscopy (JEOL 2100 with an accelerating voltage of 200 kV and a point resolution of 0.19 nm) and N_2 adsorption/desorption isotherms at −196 °C (JW–BK122F, Beijing JWGB, China). The size distribution of the catalysts was determined by measuring the edge length of >800 cubic particles for each sample.

X–ray photoelectron spectra (XPS) were recorded on an ESCALAB 250 Xi system equipped with monochromatic Al K_α (1486.6 eV) X–ray source. The binding energy of C 1s (284.8 eV) was used as an internal standard. The spectra were fitted using the XPSPEAK program by the curve fitting with the Gaussian function after subtraction of the Shirley–type background.

Raman spectra were obtained with a LabRAM HR 800 (HORIBA Jobin Yvon, France) spectrometer at room temperature and atmospheric pressure. A wavelength of 532 nm was used for the exciting source from an argon ion laser. The Laser beam was focused onto an area 0.1 × 0.1 mm^2 in size of the sample surface. The wavenumber values of the Raman spectra were accurate to 1 cm^{-1}.

H_2 temperature–programmed reduction (H_2-TPR) was carried out on a Micromeritics AutoChem II 2920. For each test, 50 mg catalyst was placed in a quartz tube and then put in contact with the reaction atmospheres. It is well known that the absorbed oxygen species generating from the reaction atmosphere (1% O_2/N_2) is crucial for the catalytic oxidation of soot [5–8], but they are not even evolved during the traditional H_2-TPR tests. Therefore, this method can only give out the catalyst reducibility roughly. To investigate the catalyst utility of O_x^{n-} more realistically, cycled TPR was performed in this work. Details of the tests are illustrated in Fig. 1, which can be described as:

- The catalyst was first pre-oxidized in 1% O_2/He at 300 °C for 10 min. Then a TPR test from −20 °C to 300 °C was performed and labeled with "O_2-". This was designed to investigate the O_x^{n-} generation ability of the catalysts [5,10].
- After this test, the samples were cooled to −20 °C without changing the atmosphere (10% H_2/Ar), another TPR was then performed and labeled with "H_2-". According to our previous study [5], the surface oxygen species observed in the "H_2-" tests can only be produced via the migration of ceria bulk oxygen to catalyst surface. This is because the catalyst surface oxygen has already been consumed by the previous "O_2-" tests, and no gaseous oxygen was introduced before the "H_2-" tests. In this sense, results of the "H_2-" tests can reveal the availability of ceria bulk oxygen over different catalysts.
- The above processes were repeated three times to test the redox stability of the catalysts, including the regeneration ability of O_x^{n-} and the utility of bulk oxygen in redox cycles. The results were denoted with "-1st", "-2nd" and "-3rd", respectively.

3. Results

3.1. Solid properties

Fig. 2 shows the X-ray diffractograms of the fresh and aged catalysts. All of them exhibit high crystallinity and a typical cubic fluoride CeO_2 crystal phase. No peak splitting can be detected for the Nd-containing catalysts, indicating the formation of solid solu-

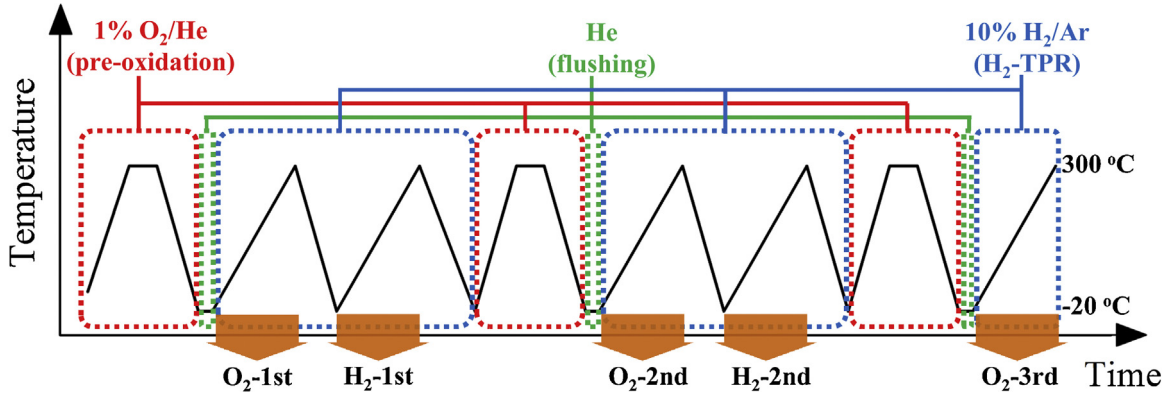

Fig. 1. Scheme of the experiments procedure of cycled TPR.

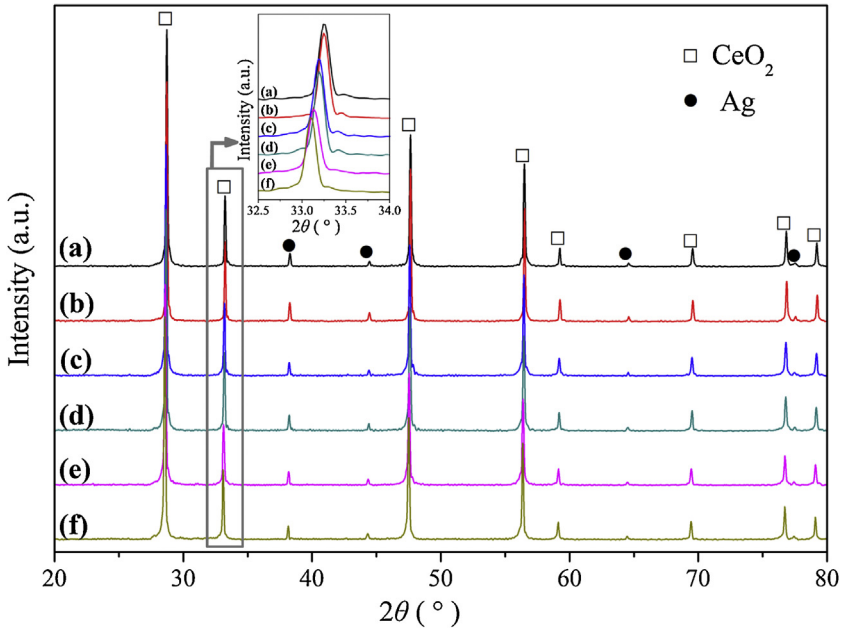

Fig. 2. XRD patterns of (a) AgCe-F, (b) AgCe-A, (c) $AgCeNd_{0.05}$-F, (d) $AgCeNd_{0.05}$-A, (e) $AgCeNd_{0.1}$-F and (f) $AgCeNd_{0.1}$-A.

tions between CeO_2 and Nd [15–17]. Moreover, the peak positions shift toward lower 2θ values with increasing Nd content, which should be attributed to the mismatch in ionic radius of Ce^{4+} (97 pm) and Nd^{3+} (112 pm). Notably, no obvious changes in peak wide and intensity are observed after ageing. This is because the fresh catalysts already exhibit high crystallinity and large crystallite sizes (see the following SEM and TEM data), then the high temperature ageing results in mainly shape transformation rather than sintering of the grains [20].

In addition to the CeO_2-derived peaks, the signals at $2\theta = 38.2^\circ$, 44.3°, 64.4° and 77.4° suggest formation of metallic silver. No evidence for the presence of Ag_2O can be obtained, both before and after ageing, which is in agreement with the results obtained by Castoldi [8], Aneggi [11], Shimizu [12] and Kayama [13] et al.

The morphology and structure of the catalysts were further explored with SEM and TEM. As shown in Fig. 3, the fresh catalysts all exhibit nanocubic morphologies with similar edge length distributions (50–400 nm). Moreover, highly dispersed metallic Ag particles (<5 nm) can be observed and evidenced by a lattice fringe of 0.24 nm (Ag{111}, see Fig. 3c, f, and i), while no AgO_x species were detected. The particle size distributions of silver agree well with the results obtained by Hu et al. [21], in which silver deposited on different CeO_{2-x}(111) thin films maintains as nanoparticles (<5 nm) at temperatures lower than 527 °C (800 K).

After ageing treatment, the geometries of AgCe-A changed from cubes to truncated cubes (and sometimes nearly spheres, see Fig. 4a and b), which agrees well with the results obtained by Aneggi et al. [20]. It is interesting to note that $AgCeNd_{0.05}$-A and $AgCeNd_{0.1}$-A are still composed of sharp-faced nanocubes, indicating the doping of Nd helps maintain the initial morphologies of the catalysts. Anyhow, when comparing Fig. 3a, d and g with Fig. 4a, d and g, respectively, it is clear that the fresh and aged catalysts share similar particle size distributions. As a consequence, it is reasonable to suggest that all the catalysts exhibit similar catalyst-soot contact conditions when mixed with soot [5].

Separately, as shown in Fig. 4b and c, Ag particles with diameter of >20 nm can be detected over AgCe-A easily [12], while large Ag particles were rarely observed on $AgCeNd_{0.05}$-A (Fig. 4f, g and h). As for $AgCeNd_{0.1}$-A, only highly dispersed Ag nanoparticles (<5 nm) can be found (Fig. 4k and l). These results imply an increased stability of Ag nanoparticles caused by Nd doping. Similar results have also been obtained by Hu et al. dealing with Ag growth behavior over Zr-doped Ag/CeO_2 thin films [22].

Textural properties of the catalysts are given in Table 1. All the fresh catalysts exhibit similar surface areas and low pore volumes

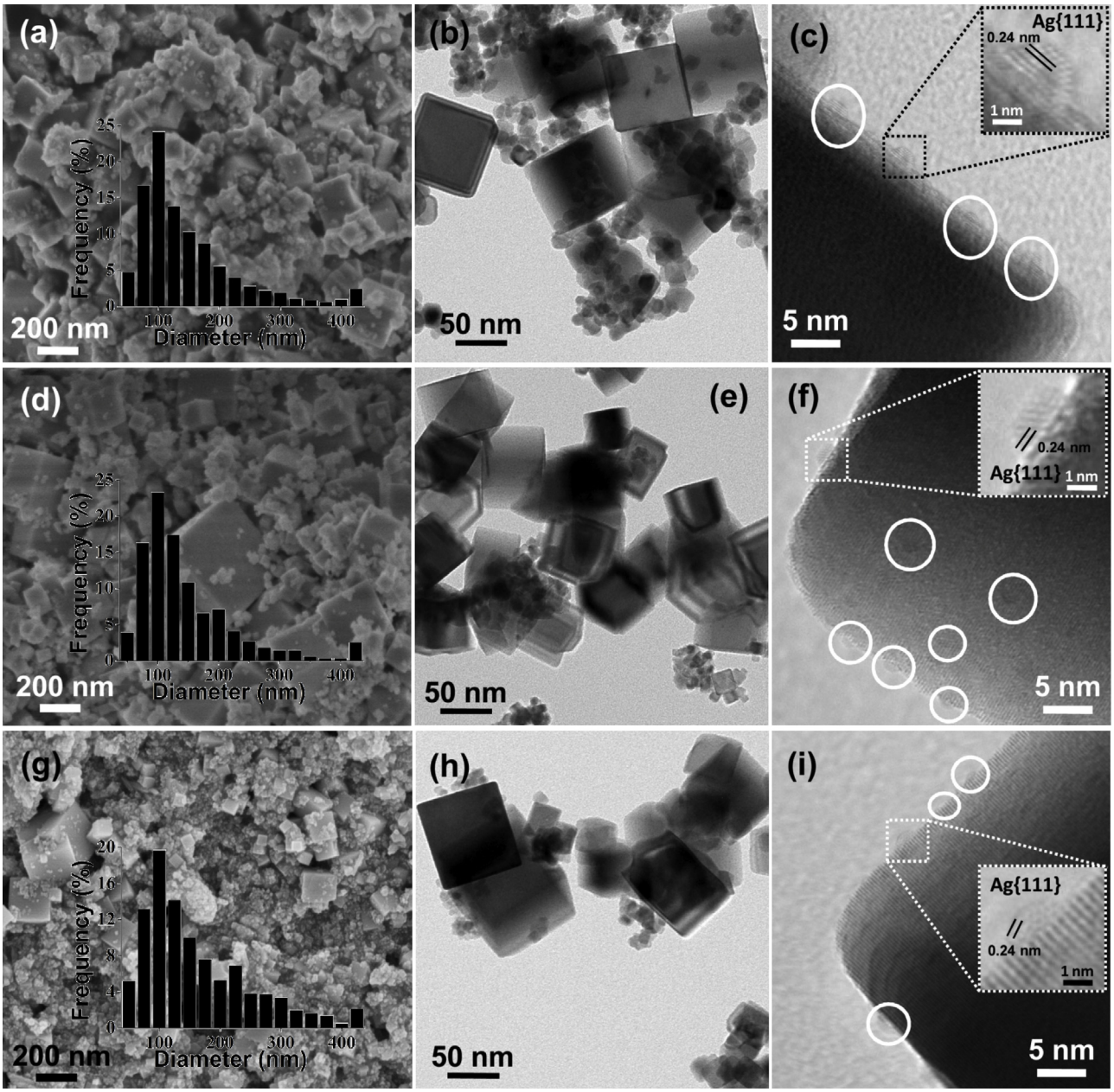

Fig. 3. Typical SEM, TEM and HRTEM images of (a–c) AgCe-F, (d–f) $AgCeNd_{0.05}$-F and (g–i) $AgCeNd_{0.1}$-F.

Table 1
Textural properties of the catalysts.

Catalyst	S_{BET} (m^2/g) [a]	Total pore volume (cm^3/g) [a]	Mesopore volume (cm^3/g) [a]	Surface Nd/Ce ratio [b]	Surface Ce^{3+}/Ce^{4+} ratio [b]	I_D/I_{F2g} [c]
AgCe-F	17.4	0.088	0.082	–	0.22	0.12
$AgCeNd_{0.05}$-F	19.1	0.117	0.111	0.37	0.27	0.11
$AgCeNd_{0.1}$-F	18.9	0.118	0.112	0.64	0.34	0.04
AgCe-A	8.8	0.036	0.033	–	0.21	0.06
$AgCeNd_{0.05}$-A	16.9	0.085	0.080	0.42	0.24	0.06
$AgCeNd_{0.1}$-A	26.6	0.130	0.124	0.70	0.30	0.06

[a] Obtained from the nitrogen physisorption at −196 °C.
[b] Obtained from the XPS data.
[c] Obtained from the Raman data.

(see Fig. 5, note the *y*-scale), indicating their nonporous structure as previously reported [5,10]. After ageing, AgCe-A experienced severe loss of its surface area, while $AgCeNd_{0.05}$-A and $AgCeNd_{0.1}$-A show no lower S_{BET} than the corresponding fresh catalysts. This can be explained by the extra mesopores that generated over these two samples (2–4 nm and 3–10 nm in size for $AgCeNd_{0.05}$-A and $AgCeNd_{0.1}$-A, respectively), which were observed distinctly by N_2 adsorption/desorption isotherms and TEM (see Fig. 5 and Fig. S1 in

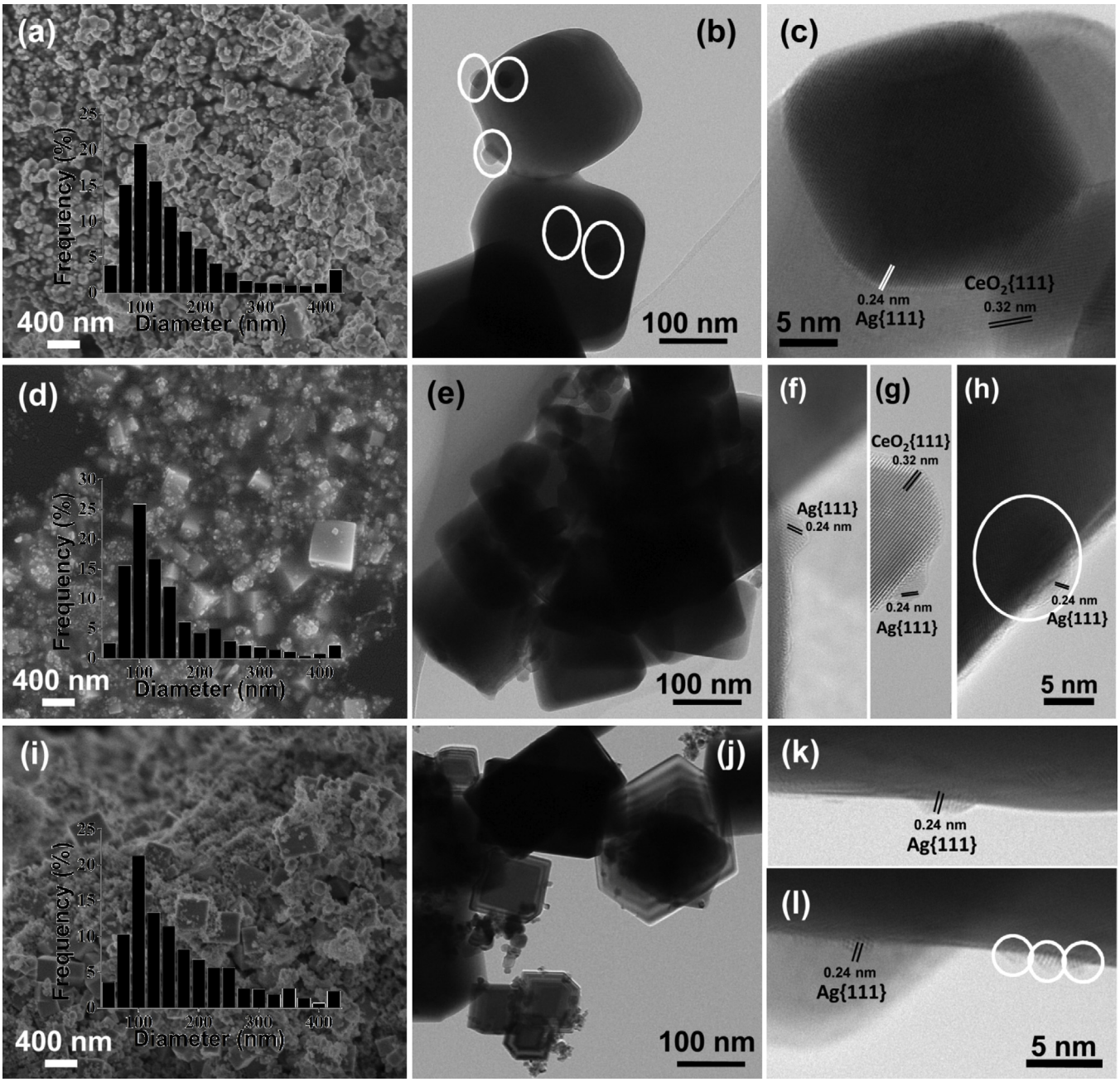

Fig. 4. Typical SEM, TEM and HRTEM images of (a–c) AgCe-A, (d–h) $AgCeNd_{0.05}$-A and (i–l) $AgCeNd_{0.1}$-A.

the Supporting information). Similar ceria mesopores generation after ageing has also been reported by Aneggi et al. [20]. Notwithstanding, since the soot particles used in this work are far larger (~25 nm in size) than these mesopores, the above changes in S_{BET} can hardly cause crucial influence on performance of the catalysts [5].

3.2. Catalyst chemical states and oxygen vacancies

In order to obtain the information of Ag chemical states and CeO_2 surface oxygen vacancies ($V_{O\text{-}s}$), XPS was performed to monitor the evolution of Ag 3d and Ce 3d spectra, the corresponding results are shown in Fig. 6 and Table 1. Some of the spectra in Fig. 6 have been normalized in intensity for a better comparison in the shapes and intensities of the peaks.

As shown in Fig. 6a, the Ag $3d_{5/2}$ binding energies of the fresh samples are at ~368.1 eV. The spectra show high symmetry and a splitting of 6 eV, implying the presence of metallic Ag [23–26]. Notably, there were controversial reports about the presence of AgO_x on CeO_2. For example, with the assistance of HRTEM, Castoldi and Aneggi et al. [8,11] indicated that both Ag metal particle and Ag_2O were present on 5 wt.% Ag/CeO_2. Nevertheless, the metallic nature of silver over Ag/CeO_2 has also been verified by many other studies via XPS, HRTEM and EXAFS [5,21–26]. As previously reported, the ceria-based supports can accelerate the decomposition of Ag_2O [27] and provide electron interaction ($Ag^+ + Ce^{3+} \rightarrow Ag^0 + Ce^{4+}$) [5,23] during catalyst synthesis, which may benefit the formation of Ag^0 rather than AgO_x. In the present work, since no evidence (XRD, HRTEM and XPS) supports the existence of AgO_x, it is suggested that metallic Ag is the dominating silver species over the fresh catalysts.

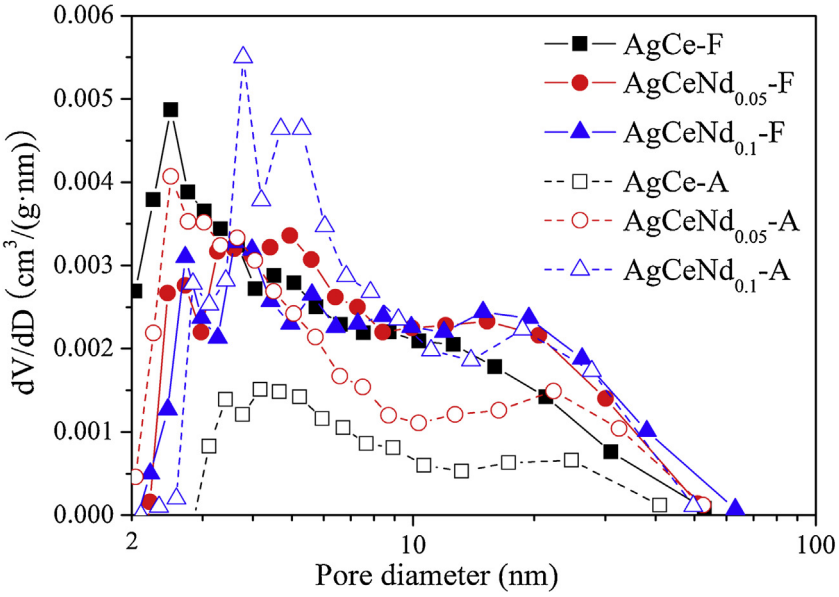

Fig. 5. Pore size distribution of the catalysts.

After annealing with 1% O_2 at 700 °C, the peaks attributed to Ag $3d_{5/2}$ and Ag $3d_{3/2}$ of Ag_2O emerged at 367.9 and 373.9 eV, respectively (Fig. 6b) [24,26], indicating that the Ag particles are partially oxidized during ageing. Based on peak deconvolution, AgCe-A exhibits slightly higher content of Ag_2O ($Ag^+/Ag^0 = 0.64$) than $AgCeNd_{0.05}$-A (0.59) and $AgCeNd_{0.1}$-A (0.57). However, these Ag_2O species can be detected by neither XRD nor HRTEM. These results imply the formation of ultra thin Ag_2O layers on the surface of Ag nanoparticles [28,29]. Since these Ag_2O species are amorphous and in small quantity, they can be detected only by surface-sensitive technique like XPS.

The surface compositions of the catalysts are given in Table 1. It is observed that the contents of surface Nd is higher than the nominal loading contents (Nd/Ce = 0.05 and 0.1 for $AgCeNd_{0.05}$-F and $AgCeNd_{0.1}$-F, respectively), implying the enrichment of Nd on catalysts' surface region. Similar surface enrichment of rare-earth metals over ceria has also been proven by many studies dealing with $Ce_xRE_{1-x}O_{2-\delta}$ (RE = La, Sm, Gd, Pr and Tb) solid solutions [30–32]. These Nd components further alter the surface oxygen vacancies ($V_{O\text{-}s}$) of Ag/CeO_2. As shown in Fig. 6c, the four satellite peaks labeled as u^0, u′, v^0 and v′ correspond to two pairs of the spin-orbit splitting doublets, which are associated with the Ce^{3+} cations [21,22]. By comparing the peak intensity of u′ and v′, it is obvious that the Ce^{3+} content of the catalysts follows an order of $AgCeNd_{0.1}$-F > $AgCeNd_{0.1}$-A > $AgCeNd_{0.05}$-F > $AgCeNd_{0.05}$-A > AgCe-F > AgCe-A, indicating Nd-doping induces the formation of Ce^{3+} [18], and the ageing treatment with 1% O_2 led to oxidation of Ce^{3+} to Ce^{4+} [33]. Considering the creation of $V_{O\text{-}s}$ is closely related with the presence of Ce^{3+} [5,10,34], it is suggested that the concentration of $V_{O\text{-}s}$ follows the same sequence for the catalysts.

Different from the surface-sensitive XPS, visible Raman spectroscopy is a useful technique to investigate the bulk oxygen vacancies ($V_{O\text{-}b}$) of the ceria-containing solid solutions [24,30–32]. As shown in Fig. 6d, all the catalysts exhibit a strong peak at ~465 cm^{-1} with a shoulder at ~600 cm^{-1}, corresponding to the F_{2g} and defect-induced (D) modes of cubic CeO_2 fluoride phase, respectively [24]. Their intensity ratios (I_D/I_{F2g}) in Table 1 indicate that the loading of 10% Nd reduced the $V_{O\text{-}b}$ concentration of Ag/CeO_2 obviously. This means Nd doping affects the creation of $V_{O\text{-}b}$ in a different way to that of $V_{O\text{-}s}$. Possible explanations are as follows: during catalyst synthesis, Ag species over ceria leads to oxygen reverse spillover [5,21,22], which creates $V_{O\text{-}s}$ that re-filled rapidly by bulk oxygen of CeO_2 via diffusion. Consequently, Ag promotes the generation of $V_{O\text{-}b}$ rather than $V_{O\text{-}s}$ [24]. With the loading of Nd, excessive $V_{O\text{-}s}$ increases the adsorption energies of O-Ce, and hereby makes oxygen reverse spillover from CeO_2 to silver difficult [35]. Therefore, $Ag/Ce_xNd_{1-x}O_2$ cannot generate $V_{O\text{-}b}$ as readily as Ag/CeO_2. A similar "obstruction" effect of Pr doping on Pd-Ce interaction and oxygen reverse spillover has been reported by Ran et al. [36].

Separately, according to the results obtained by Chueh et al. [37], bulk Ce^{3+} can be oxidized by gaseous O_2 even more easily than surface Ce^{3+}. Therefore, ageing treatment in 1% O_2 reconciled the $V_{O\text{-}b}$ concentration of all the catalysts to a similar low level (Table 1).

3.3. Catalytic activities for soot oxidation

Fig. 7 illustrates the catalytic performance of the samples, all the catalysts yield a high CO_2 selectivity during the reactions (CO_2/CO_x > 99%). As shown in Fig. 7a, T_{max} (maximal soot oxidation rate temperature) of the catalysts follows an order of AgCe-F (394 °C) < $AgCeNd_{0.05}$-F (413 °C) < $AgCeNd_{0.05}$-A (439 °C) < AgCe-A (448 °C) < $AgCeNd_{0.1}$-F (455 °C) ≈ $AgCeNd_{0.1}$-A (458 °C), suggesting that the introduction of Nd decreases the activity of Ag/CeO_2, but increases its thermal stability instead. Notably, the sharp CO_2 peak of AgCe-A indicates thermal runaway over this catalyst, which may lead to inaccurate presentation of the catalyst soot oxidation activity [38]. Therefore, it is necessary to re-evaluate the catalyst performance via isothermal reactions. Moreover, considering there is always a certain amount of water vapor in the exhaust of GPF [3], the influence of water to the catalytic performance of AgCe-F was evaluated by introducing 10% H_2O during soot-TPO test. As shown in Fig. S2 in the Supporting information, water seems to benefit the oxidation of soot slightly, which has once been attributed to the elimination of adsorbed hydrogen by oxygen species and the increase in contact area caused by gasification of carbon with water [39]. Nevertheless, since these changes in catalyst activity are rather small (especially at temperatures below 320 °C), and most of the important characterizations applied in this study (e.g. TEM, XPS, Raman and especially H_2-TPR) cannot be performed in a humid atmosphere, thus the following results and discussion are made based on soot oxidation reactions in absence of water.

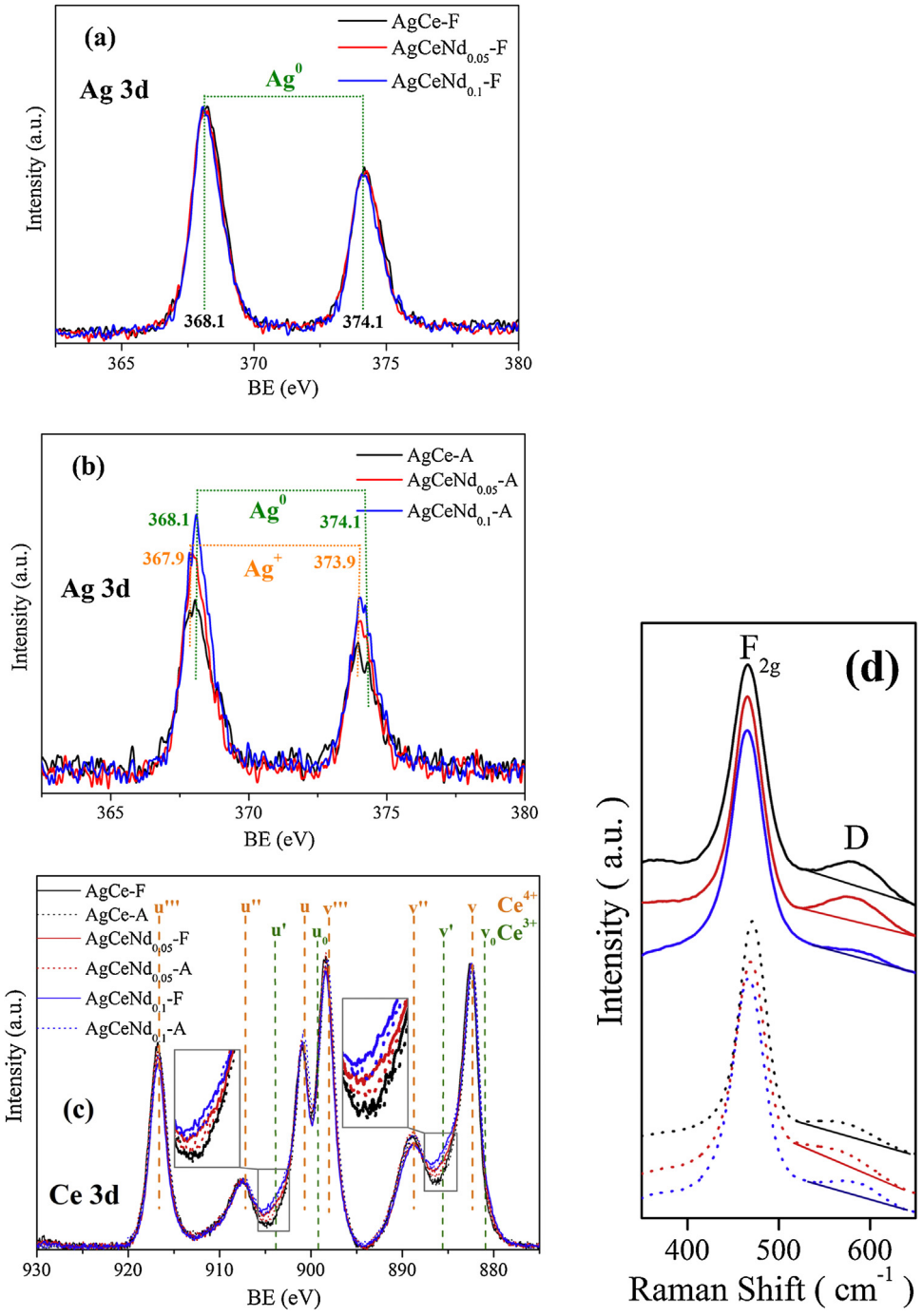

Fig. 6. (a-c) XPS and (d) Visible Raman spectra of the catalysts in the (a,b) Ag 3d and (c) Ce 3d core level regions. Fig. 6c and d share the same legend.

The results of isothermal soot oxidation were shown in Fig. 7b. It is noted that, since soot conversion of AgCe-F and $AgCeNd_{0.05}$-F at 350 °C is relatively high (>10%), not only catalyst deactivation, but also changes in soot remaining amount may cause the drop in CO_2 production over these catalysts. Meanwhile, the reactions at 300 °C were in a more stable state, which could thus reflect the behavior of the catalysts more accurately. Similar attention should be paid when analyze the catalytic performance of all the aged catalysts at 400 °C.

Among the fresh catalysts, AgCe-F exhibits the highest reaction rate, following by $AgCeNd_{0.05}$-F and $AgCeNd_{0.1}$-F. All of them exhibited time on-stream deactivation, which was attributed to insufficient O_x^- supplement in our previous works [5,10]. It is noteworthy that, no deactivation was observed over AgCe-F when the reactions are performed in "tight-contact" conditions (not shown), indicating the lack of catalyst-soot contact points in "loose-contact" conditions makes O_x^- supplement even more difficult. After ageing, the catalysts are almost inert at 300 °C. When the temperature was raised to 350 and 400 °C, $AgCeNd_{0.05}$-A followed by $AgCeNd_{0.1}$-A exhibits obviously better activities than AgCe-A. Interestingly, $AgCeNd_{0.1}$-A shows no worse catalytic performance than $AgCeNd_{0.1}$-F at 350 °C, which again confirms that Nd doping improves the stability of Ag/CeO_2.

3.4. Cycled H_2 temperature–programmed reduction

As reported earlier [5–10,14], surface oxygen species (O_x^{n-}) are the main active phases for soot oxidation over ceria-based catalysts,

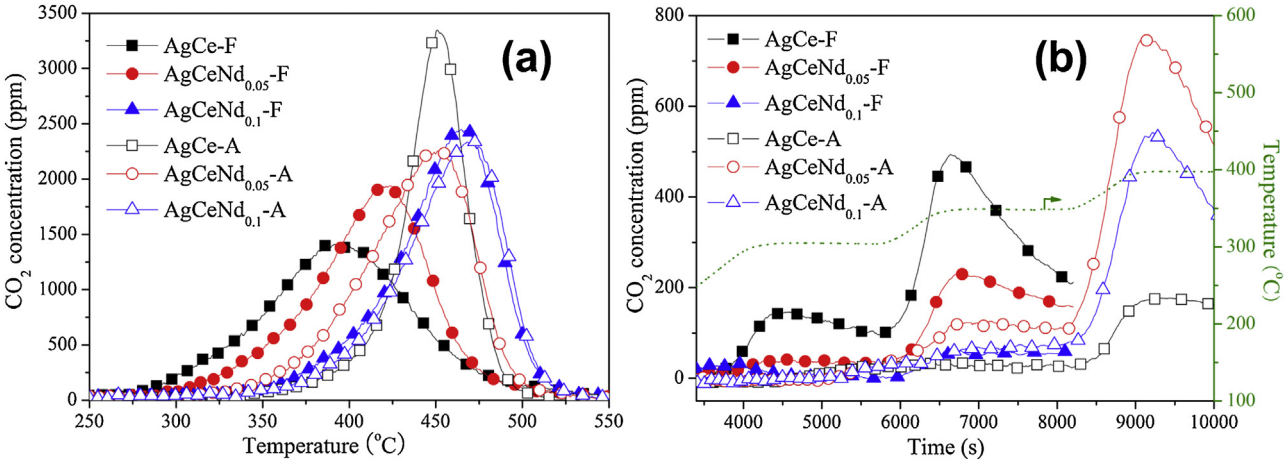

Fig. 7. CO_2 concentration during (a) temperature-programmed and (b) isothermal soot oxidation reactions. Reaction conditions: 1% O_2/N_2 (500 mL/min), catalyst/soot = 10/1, loose contact, heating rate = 5 °C/min.

and H_2-TPR is an efficient method to investigate the catalyst utility of O_x^{n-}. With the assistance of silver, these species can be consumed by H_2 at <300 °C (see Fig. S3 in the Supporting information) [5]. Therefore, each cycled TPR test was terminated at 300 °C to ensure that most of O_x^{n-} can be consumed, while no obvious structural changes of the catalysts are expected since all the catalysts were synthesized via calcinations at ≥500 °C.

As illustrated in Fig. 8a, the H_2 consumption peaks at 0–40 °C, 50–70 °C and 100–240 °C over AgCe-F become distinct after pre-oxidation (comparing with the profiles in Fig. S3). According to our previous studies [5,23], these peaks can be assigned to reduction of surface-adsorbed O_2^-, O^- and surface capping oxygen (O^{2-}), respectively. After carefully dealing with the profiles' baselines (see Fig. S4a in the Supporting information for details), quantitative data were obtained and shown in Table 2. Based on the discussion in Section 2.3, the cycled H_2-TPR results can be analyzed in three parts: (1) the "O_2-" data concerning about catalyst O_x^{n-} generation ability, (2) the "H_2-" data concerning about catalyst availability of ceria bulk oxygen and (3) differences between the "-1st", "-2nd" and "-3rd" data, which reflect catalyst redox stability and O_x^{n-} regeneration.

(1) For the fresh catalysts, $AgCeNd_{0.05}$-F and $AgCeNd_{0.1}$-F exhibit significantly lower amount of O_2^- than AgCe-F in the "O_2-" tests (see Fig. 8b, c and Table 2). Their O^- and O^{2-}-derived H_2 consumption peaks become overlapped, and the proportion of O^{2-} goes up remarkably with Nd content. These results were reconfirmed by Raman (see Fig. S4b), indicating excessive $V_{O\text{-}s}$ induces the formation of less active oxygen species (like O^{2-}) rather than O_2^- [5,10]. After ageing, the amount of O_x^- (especially O_2^-) generated over AgCe-A was reduced drastically compared with AgCe-F (Fig. 8d and Table 2). Meanwhile, $AgCeNd_{0.05}$-A and $AgCeNd_{0.1}$-A exhibit even higher content of O_2^- than the corresponding fresh catalysts (see Fig. 8e, f and Table 2). Considering O_2^- is highly active for soot catalytic oxidation [5–7,13], these results explain why ageing treatment caused less impact on the Nd-containing catalysts.

Notably, H_2 consumption occurred at higher temperatures over $AgCeNd_{0.05}$-A and especially AgCe-A compared with the fresh catalysts (comparing Fig. 8a and b with Fig. 8d and e, respectively). This is because sintering of the Ag nanoparticles decreased their active surface area for H_2 adsorption and spillover. Separately, $AgCeNd_{0.1}$-A and $AgCeNd_{0.1}$-F show similar H_2 reduction temperatures, which reconfirms the Ag stabilization effect caused by Nd doping.

(2) As indicated in Section 2.3, the surface oxygen species observed in H_2–1st and 2nd TPRs of AgCe-F can only be produced via the migration of ceria bulk (mainly subsurface [40]) oxygen to catalyst surface. This process was proven accelerated by the participant of silver through a reverse spillover effect [5,21,22]. As shown in Table 2, the amount of bulk oxygen-derived O_x^- species (H_2-1st) can be comparable to the gaseous O_2-derived O_x^- (O_2-1st). In this sense, the bulk-to-surface migration of oxygen plays important role during soot oxidation over AgCe-F.

Meanwhile, as evidenced by the H_2–1st and –2nd results, the migration of bulk oxygen to catalyst surface was inhibited by Nd doping (especially for $AgCeNd_{0.1}$-F, see Fig. 8c). This is mainly because the loading of Nd reduces $V_{O\text{-}b}$ of CeO_2 (see Table 1 and Fig. 6d), which hereby decreases the oxygen diffusion rate in ceria bulk [34]. Moreover, since excessive $V_{O\text{-}s}$ inhibits the oxygen reverse spillover from CeO_2 to Ag [35], $AgCeNd_{0.05}$-F shows less availability of ceria bulk oxygen than AgCe-F (see the "H_2-1st" results in Fig. 8a, b and Table 2) although they exhibit similar content of $V_{O\text{-}b}$ (Table 1).

After ageing, the availability of bulk oxygen over AgCe-A becomes negligible due to severe Ag sintering (Fig. 8d and Table 2). Contrarily, $AgCeNd_{0.05}$-A and $AgCeNd_{0.1}$-A with high thermal stability can still produce O_x^- with ceria bulk oxygen (Fig. 8e, f and Table 2).

(3) By comparing the O_2-1st, 2nd and 3rd results of AgCe-F (Table 2), it is clear that the amount of active oxygen species (O_x^-) drops obviously during the redox cycles. In this sense, during soot oxidation in 1% O_2 at 300 °C, once the O_x^- species over AgCe-F are consumed by soot, they can hardly be regenerated by gaseous O_2 immediately (not even in minutes, as the pre-oxidation process lasts for 10 min). Therefore, it is reasonable to speculate the deficient redox stability of AgCe-F leads to its time-on-stream deactivation. As shown in Fig. 7b, 8b, 8c and 8d, similar redox instability and deactivation can also be observed over $AgCeNd_{0.05}$-F, $AgCeNd_{0.1}$-F and AgCe-A. Nevertheless, $AgCeNd_{0.05}$-A and especially $AgCeNd_{0.1}$-A exhibit even better redox stability after ageing (Table 2). This is because they have similar Ag particle sizes but lower $V_{O\text{-}s}$ contents compared with the fresh catalysts.

By comparing the H_2–1st and 2nd results, it is observed that the bulk oxygen-derived O_x^{n-} is quite stable during the redox cycles, which indicates that ceria bulk oxygen plays important role in maintaining stable catalytic cycles. Consequently, as shown in Fig. 7b (300 °C for the fresh catalysts, 350 °C for the aged ones), the catalysts first deactivated with time on stream, then reached stable activities during isothermal soot oxidation.

As a summary, Nd doping inhibits the formation of highly active surface oxygen species and thus leads to a low initial soot oxidation activity. However, the capability to maintain certain O_x^- generation

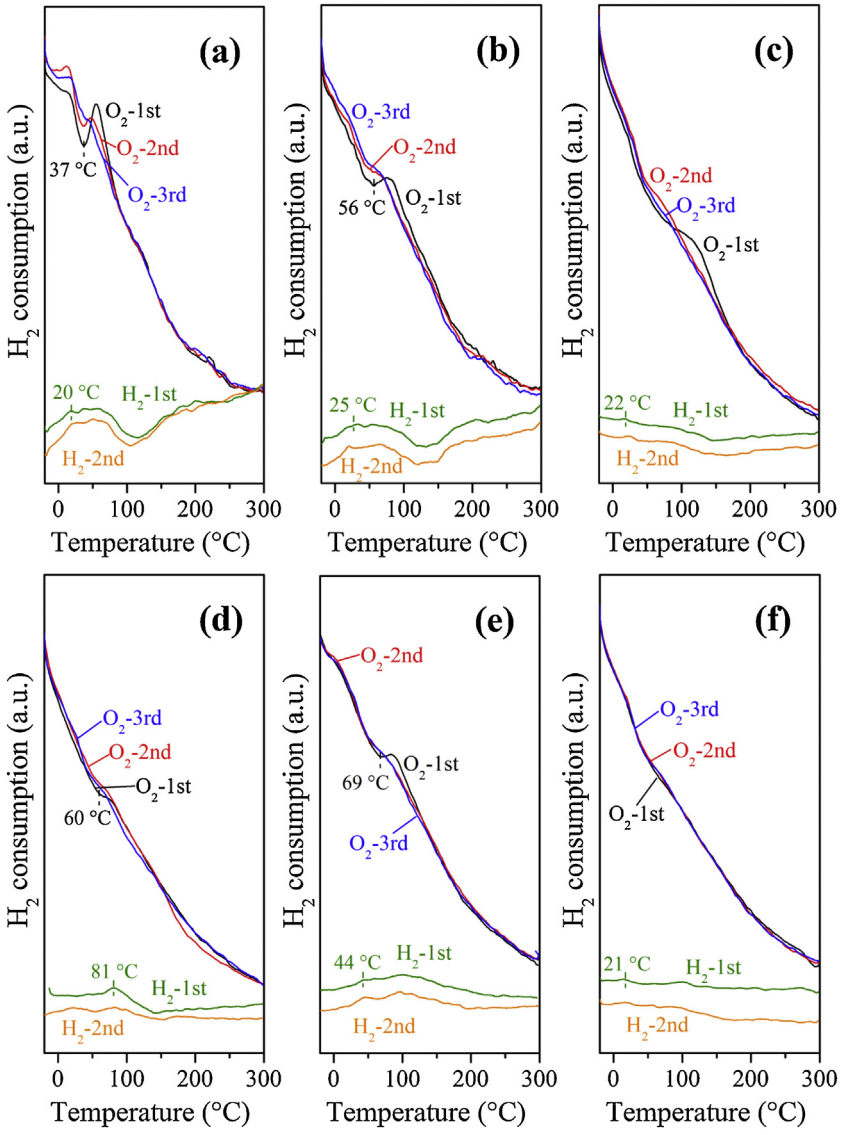

Fig. 8. Cycled TPR results of (a) AgCe-F, (b) $AgCeNd_{0.05}$-F, (c) $AgCeNd_{0.1}$-F, (d) AgCe-A, (e) $AgCeNd_{0.05}$-A and (f) $AgCeNd_{0.1}$-A.

Table 2
Quantitative analyses of the surface oxygen species-derived H_2 consumptions ($\mu mol/g_{catal.}$) in cycled-TPR.

Catalyst	O_2-1st			O_2-2nd			O_2-3rd			H_2-1st		H_2-2nd	
	O_2^-	O^-	O^{2-}	O_2^-	O^-	O^{2-}	O_2^-	O^-	O^{2-}	O_x^-	O^{2-}	O_x^-	O^{2-}
AgCe-F	4.5	18.1	1.5	5.2	9.2	1.9	2.6	3.3	1.9	20.7	8.4	21.5	6.3
$AgCeNd_{0.05}$-F	1.5	23.5 (o) [a]		1.1	14.2 (o)		0.9	11.1 (o)		17.4	5.2	19.0	3.1
$AgCeNd_{0.1}$-F	0.5	27.3 (o)		0.3	9.6 (o)		0.3	5.2 (o)		5.0	1.4	4.7	1.3
AgCe-A	0	8.0 (o)		0	12.0 (o)		0.1	3.1 (o)		15.8 (o)		15.1 (o)	
$AgCeNd_{0.05}$-A	2.1	23.1 (o)		2.2	10.1 (o)		1.7	9.4 (o)		17.9 (o)		18.4 (o)	
$AgCeNd_{0.1}$-A	0.5	3.6 (o)		0.6	5.1 (o)		0.5	5.1 (o)		5.8 (o)		6.2 (o)	

[a] (o) means these peaks overlapped.

(from gaseous O_2 or ceria bulk oxygen) even after high-temperature ageing makes $Ag/Ce_xNd_{1-x}O_2$ more thermally stable than Ag/CeO_2.

4. Discussion

In reviewing of soot oxidation mechanisms over ceria-based catalysts, surface oxygen species (O_x^{n-}) have been proven as the most important active phases [5–10,14]. During a typical reaction, once these species were consumed by soot, they should be regenerated with gaseous O_2 and/or ceria bulk oxygen, and thus maintain a stable catalytic cycle (a Mars-van-Krevelen-like mechanism). For Ag/CeO_2, there are mainly three factors that may influence the catalytic cycle. (1) Catalyst morphologies can alter the number of catalyst-soot contact points, and then determine the transfer efficiency of O_x^{n-} from catalyst to soot [5,9,40]. (2) The particle size and chemical states of Ag are closely related with both the dissociation of gaseous O_2 and utility of ceria bulk oxygen [41], which are crucial for the generation of O_x^{n-}. (3) The concentration of oxygen vacancies (both $V_{O\text{-}s}$ and $V_{O\text{-}b}$) was proven associated with the amount and specific type of O_x^{n-} (O_2^-, O^- and/or O^{2-}) [5,7,10],

while the interaction between oxygen vacancies and Ag may further impact the catalytic and thermal behaviors of Ag [21,22,40]. In this sense, the following discussions were made upon (1) how Nd doping influences the above three factors, and (2) how the influenced factors further affect the entire catalytic cycle and catalyst activity. The fresh and aged catalysts were discussed separately for comparison.

4.1. Effect of Nd doping on the fresh catalysts

As evidenced by HRTEM, XPS and SEM, the three fresh catalysts exhibit similar catalyst morphologies (nanocubes, see Fig. 3), Ag particle sizes (<5 nm, see Fig. 3) and chemical states (Ag^0, see Fig. 6b). Meanwhile, as evidenced by XRD (Fig. 2), XPS (Fig. 6c) and Raman (Fig. 6d), the substitution of CeO_2 with trivalent Nd^{3+} ions results in formation of ceria-based solid solutions accompanied with generation of more $V_{O\text{-}s}$ and less $V_{O\text{-}b}$. Therefore, factor (3) (the concentration of oxygen vacancies) domains the differences between AgCe-F, $AgCeNd_{0.05}$-F and $AgCeNd_{0.1}$-F. The influences of $V_{O\text{-}s}$ and $V_{O\text{-}b}$ on O_x^{n-} should thus be paid close attention to.

On one hand, $V_{O\text{-}s}$ is closely related with the gaseous oxygen-derived O_x^{n-}. Over Ag/CeO_2, O_2 is transformed into O_x^{n-} via: $O_2(g) \rightarrow 2O(+e) \rightarrow O_2^-(+e) \rightarrow 2O^-(+2e) \rightarrow 2O^{2-}$ [5,7,23,35]. During the first adsorption and dissociation processes ($O_2 \rightarrow 2O$), $V_{O\text{-}s}$ favors the formation of atomic O. This has been evidenced by first-principles calculations [35] and the O_2–1st TPR results in this work, in which $AgCeNd_{0.1}$-F exhibits higher surface oxygen-derived H_2 consumption (27.8 μmol/$g_{catal.}$) than $AgCeNd_{0.05}$-F (25.0 μmol/$g_{catal.}$) and AgCe-F (24.1 μmol/$g_{catal.}$). However, during the subsequent transformation processes ($2O \rightarrow O_2^- \rightarrow 2O^- \rightarrow 2O^{2-}$), excessive $V_{O\text{-}s}$ and Ce^{3+} lead to deep reduction of the oxygen. As a consequence, although Nd doping accelerates O_x^{n-} formation, it favors the formation of O^{2-} instead of the highly active O_x^- (Table 2) [5,7].

On the other hand, both $V_{O\text{-}b}$ and $V_{O\text{-}s}$ are crucial for the bulk oxygen-derived O_x^{n-}. Under reduction conditions (e.g. when catalyst reacts with H_2 or soot), atomic oxygen (O) can release from ceria bulk and transform into surface O_x^{n-} through: $O^{2-}(bulk) \rightarrow 2O \rightarrow O_2^- \rightarrow 2O^- \rightarrow 2O^{2-}$ [5,34,40]. The first step ($O^{2-}(bulk) \rightarrow 2O$) determines the catalyst utility of bulk oxygen, which can be improved by a high content of $V_{O\text{-}b}$ and the reverse spillover of oxygen from CeO_2 to Ag [5,21,22,34]. However, as indicated in Sections 3.2 and 3.4, due to the reduced $V_{O\text{-}b}$ (Fig. 6d) and extra $V_{O\text{-}s}$ (Fig. 6c) caused by Nd doping, both the steps were inhibited over $Ag/Ce_xNd_{1-x}O_2$. As a consequence, the bulk oxygen in $AgCeNd_{0.05}$-F and especially $AgCeNd_{0.1}$-F cannot be fully utilized to generate surface O_x^{n-}, which is supported clearly by the suppressed H_2 consumption during H_2–1st and –2nd TPRs of $AgCeNd_{0.1}$-F (Fig. 8c).

As a summary, since the doping of Nd inhibits the availability of ceria bulk oxygen, and induces the formation of less active oxygen species as well, $Ag/Ce_xNd_{1-x}O_2$ can hardly provide enough active species during the reaction and regeneration processes. Therefore, it is not surprising that both $AgCeNd_{0.05}$-F and $AgCeNd_{0.1}$-F exhibit far lower soot oxidation activity than AgCe-F (Fig. 7b).

4.2. Effect of Nd doping on the aged catalysts

To understand the influences of Nd additives on the aged catalysts, one should first be aware of the roles that Nd species played during ageing. As previously mentioned, although the morphologies of AgCe-A (cubes, truncated cubes and spheres, see Fig. 4a and b) are slightly different from the Nd-doping catalysts (cubes, see Fig. 4d, e, i and j), their identical particle size distributions imply similar catalyst-soot contact conditions [5]. In this sense, only factor (2) (Ag particle size and chemical states) and factor (3) (the concentration of oxygen vacancies) were concerned in the following discussions.

First, about the particle sizes of Ag: as illustrated in Table 1, Fig. 5 and Fig. S1 (see the Supporting information), both $AgCeNd_{0.05}$-A and $AgCeNd_{0.1}$-A generate extra mesopores during ageing, resulting in their higher S_{BET} compared with AgCe-A. Although these mesopores contribute little to soot catalytic oxidation [5], they led to isolation of the primary Ag nanoparticles and hereby hampered silver migration upon aging [42]. Furthermore, Hu et al. [21,22] have proven that surface oxygen vacancies increase the bonding of Ag to the ceria surface, which implies that the excessive $V_{O\text{-}s}$ over $Ag/Ce_xNd_{1-x}O_2$ catalysts may help inhibit Ag sintering. In either case, the Ag nanoparticles over $Ag/Ce_xNd_{1-x}O_2$ are far more stable than those over Ag/CeO_2, which was evidenced by the HRTEM (Fig. 4) and H_2-TPR (Fig. 8) results.

The sintering of Ag can affect the catalytic oxidation of soot significantly. For example, Shimizu [12] and Haneda et al. [43] found that large Ag particles (>15 nm) supported on CeO_2, ZrO_2, TiO_2 and MgO showed obviously worse soot oxidation activities than Ag nanoparticles (<5 nm). Their low activity has been attributed to the decrease in Ag surface area and hereby weakened O_2 activation ability [41]. This was also evidenced by the H_2-TPR results in this work: as shown in Fig. 8d and Table 2, AgCe-A can hardly generate any O_2^- during O_2-1st, 2nd and 3rd TPRs. Contrarily, $AgCeNd_{0.05}$-A and $AgCeNd_{0.1}$-A generates no less O_x^- than the corresponding fresh catalysts, indicating the Ag nanoparticles over their surface can still work well to adsorb and activate gaseous O_2. What's more, Ag sintering leads to loss of CeO_2-Ag contact, which impacts the bulk-to-surface migration of oxygen. As confirmed by the H_2–1st and 2nd TPR results (Table 2), $AgCeNd_{0.05}$-A and especially AgCe-A generates less bulk oxygen-derived O_x^- species compared with the corresponding fresh catalysts, while there are no obvious differences between $AgCeNd_{0.1}$-A and $AgCeNd_{0.1}$-F (Fig. 8c and f).

On all accounts, sintering of Ag reduces the catalyst availability for active oxygen (both from gaseous O_2 and ceria bulk oxygen), which thus reduces the soot oxidation activity of AgCe-A drastically. Meanwhile, Nd doping restrains Ag particle growth and hereby improves the catalyst stability towards thermal ageing.

Second, about the chemical states of Ag: as indicated by the XPS results (Fig. 6b and c), AgCe-A exhibits slightly higher content of Ag_2O than $AgCeNd_{0.05}$-A and $AgCeNd_{0.1}$-A, which may be attributed to more remarkable oxygen reverse spillover on Ag/CeO_2 as mentioned above. Anyhow, these differences in Ag chemical states should not be crucial for the catalytic reaction, the reasons are twofold: On one hand, the amount of these Ag_2O is very low (they cannot be detected either by XRD or HRTEM). Furthermore, AgCe-A with higher content of Ag_2O shows no more H_2 consumption than $AgCeNd_{0.05}$-A (see O_2–1st in Fig. 8d and e), which also implies a limited contribution of the surface Ag_2O species to the catalytic reaction. On the other hand, as evidenced by Haneda [43] and Corro et al. [44], during soot oxidation, Ag_2O can act as the oxidizing agent which gets reduced readily by soot to form metallic Ag. Therefore, it is also impossible for the Ag_2O species to persist and do continuous influence on the reaction. In a word, the differences in silver chemical states cannot determine the catalytic cycle.

Finally, about the concentration of oxygen vacancies: ageing treatment with 1% O_2 led to oxidation of Ce^{3+} to Ce^{4+} over all the catalysts (Fig. 6c and d). With reduction of $V_{O\text{-}s}$, $AgCeNd_{0.05}$-A and $AgCeNd_{0.1}$-A generated higher amounts of O_2^- during O_2-1st, 2nd and 3rd tests than corresponding fresh catalysts (Table 2) [5,10]. Separately, decrease in $V_{O\text{-}b}$ content hamper the utility of ceria bulk oxygen over $AgCeNd_{0.05}$-A obviously (comparing the H_2–1st results in Fig. 8b and e). As for AgCe-A, the influences of Ag sintering and $V_{O\text{-}b}$ reduction overwhelms that of $V_{O\text{-}s}$ decrease, making this catalyst hardly available for active oxygen and the least active among the aged catalysts.

As a summary, we consider the changes in Ag particle sizes are the most important factors that determine the catalytic behavior of the aged catalysts. Nd doping inhibits the growth of Ag, and thus improves the catalyst stability at high temperatures. Although reduction in $V_{O\text{-}s}$ may benefit the catalytic performance, its influences can be shadowed by Ag sintering. Consequently, AgCe-A with severe Ag sintering is almost inert for soot oxidation. Meanwhile, $AgCeNd_{0.05}$-A suffered from decrease in bulk-to-surface oxygen migration caused by $V_{O\text{-}b}$ reduction. As for $AgCeNd_{0.1}$-A, it exhibits reduced $V_{O\text{-}s}$ amount, increased $V_{O\text{-}b}$ content and unchanged Ag particle sizes comparing with $AgCeNd_{0.1}$-F, and thus shows no deactivation even after ageing (see Fig. 7b).

5. Conclusions

In this study, by characterization and comparison of three cubic $Ag/Ce_xNd_{1-x}O_2$ catalysts, several conclusions can be drawn:

- Both activation of gaseous O_2 and oxygen bulk-to-surface migration were confirmed to play important roles in soot catalytic oxidation over Ag/CeO_2 catalysts. Any changes in catalyst structure may affect these two factors, and thus alter the catalyst performance.
- Nd doping increases surface oxygen vacancies ($V_{O\text{-}s}$), but decreases bulk oxygen vacancies ($V_{O\text{-}b}$) over Ag/CeO_2. This suppresses the utilization of ceria bulk oxygen, and induces the formation of less active O_2^- species instead of O_2^-, resulting in reduction of the soot oxidation activity.
- The surface oxygen vacancies and mesopores in the ceria support generated via Nd doping inhibit Ag sintering at high temperatures, which hereby improves the catalyst stability towards high-temperature ageing effectively.

Based on these conclusions, it is suggested that cubic Ag/CeO_2 catalysts can be more practical with the introduction of Nd. However, the Nd doping amount should be controlled moderately to ensure both the activity and thermal stability of $Ag/Ce_xNd_{1-x}O_2$. Under the specific conditions applied in this work, the optimal Nd loading is 5%.

Acknowledgements

The authors would like to acknowledge Project 2015AA034603 by the Ministry of Science and Technology of China, China Postdoctoral Science Foundation (2015M580607), Project 113007A by the Ministry of Education of China and the Fundamental Research Funds for the Central Universities. Moreover, we would also thank the financial support from the Key Laboratory of Advanced Materials of Ministry of Education of China.

Appendix A. Supplementary data

Supplementary data associated with this article can be found, in the online version, at http://dx.doi.org/10.1016/j.apcatb.2016.10.006.

References

[1] Y. Kameya, K.O. Lee, J. Nanopart. Res. 15 (2013) 2006.
[2] T. Boger, D. Rose, P. Nicolin, N. Gunasekaran, T. Glasson, Emiss. Control Sci. Technol. 1 (2015) 49–63.
[3] D. Lopez-Gonzalez, M.N. Tsampas, A. Boréave, L. Retailleau-Mevel, M. Klotz, C. Tardivat, B. Cartoixa, K. Pajot, P. Vernoux, Top. Catal. 58 (2015) 1242–1255.
[4] T. Johnson, Vehicular emissions in review: SAE Technical Series Paper 2014-01-1491 (2014).
[5] S. Liu, X. Wu, W. Liu, W. Chen, R. Ran, M. Li, D. Weng, J. Catal. 337 (2016) 188–198.
[6] S. Liu, X. Wu, D. Weng, R. Ran, J. Rare Earth 33 (2015) 567–590.
[7] M. Machida, Y. Murata, K. Kishikawa, D. Zhang, K. Ikeue, Chem. Mater. 20 (2008) 4489–4494.
[8] L. Castoldi, E. Aneggi, R. Matarrese, R. Bonzi, J. Llorca, A. Trovarelli, L. Lietti, Catal. Today 258 (2015) 405–415.
[9] M. Piumetti, S. Bensaid, N. Russo, D. Fino, Appl. Catal., B 165 (2015) 742–751.
[10] S. Liu, X. Wu, J. Tang, P. Cui, X. Jiang, C. Chang, W. Liu, Y. Gao, M. Li, D. Weng, Catal. Today (2016) http://dx.doi.org/10.1016/j.cattod.2016.05.036.
[11] E. Aneggi, J. Llorca, C. de Leitenburg, G. Dolcetti, A. Trovarelli, Appl. Catal., B 91 (2009) 489–498.
[12] K. Shimizu, M. Katagiri, S. Satokawa, A. Satsuma, Appl. Catal., B 108–109 (2011) 39–46.
[13] T. Kayama, K. Yamazaki, H. Shinjoh, J. Am. Chem. Soc. 132 (2010) 13154–13155.
[14] A. Bueno-López, Appl. Catal., B 146 (2014) 1–11.
[15] A.M. Hernández-Giménez, L.P. dos Santos Xavier, A. Bueno-López, Appl. Catal., A 462–463 (2013) 100–106.
[16] A.M. Hernández-Giménez, D. Lozano-Castelló, A. Bueno-López, Appl. Catal., B 148–149 (2014) 406–414.
[17] L.P. dos Santos Xavier, V. Rico-Pérez, A.M. Hernández-Giménez, D. Lozano-Castelló, A. Bueno-López, Appl. Catal., B 162 (2015) 412–419.
[18] N. Shehata, K. Meehan, M. Hudait, N. Jain, J. Nanopart. Res. 14 (2012) 1173.
[19] L. Wang, J.R. Gaudet, W. Li, D. Weng, J. Catal. 306 (2013) 68–77.
[20] E. Aneggi, D. Wiater, C. Leitenburg, J. Llorca, A. Trovarelli, ACS Catal. 4 (2014) 172–181.
[21] S. Hu, Y. Wang, W. Wang, Y. Han, Q. Fan, X. Feng, Q. Xu, J. Zhu, J. Phys. Chem. C 119 (2015) 3579–3588.
[22] S. Hu, W. Wang, Y. Wang, Q. Xu, J. Zhu, J. Phys. Chem. C 119 (2015) 18257–18266.
[23] J. Zhang, L. Li, X. Huang, G. Li, J. Mater. Chem. 22 (2012) 10480–10487.
[24] S. Chang, M. Li, Q. Hua, L. Zhang, Y. Ma, B. Ye, W. Huang, J. Catal. 293 (2012) 195–204.
[25] C. Lee, J. Park, Y. Shul, H. Einaga, Y. Teraoka, Appl. Catal., B 174 (2015) 185–192.
[26] F. Benedetti, P. Luches, M.C. Spadaro, G. Gasperi, S. D'Addato, S. Valeri, F. Boscherini, J. Phys. Chem. C 119 (2015) 6024–6032.
[27] S. Imamura, H. Yamada, K. Utani, Appl. Catal., A 192 (2000) 221–226.
[28] H. Bi, W. Cai, C. Kan, L. Zhang, D. Martin, F. Träger, J. Appl. Phys. 92 (2002) 7491–7497.
[29] B. Aswathy, G.S. Avadhani, I.S. Sumithra, S. Suji, G. Sony, J. Mol. Liq. 159 (2011) 165–169.
[30] M. Luo, Z. Yan, L. Jin, M. He, J. Phys. Chem. B 110 (2006) 13068–13071.
[31] M. Guo, J. Lu, Y. Wu, Y. Wang, M. Luo, Langmuir 27 (2011) 3872–3877.
[32] B.M. Reddy, L. Katta, G. Thrimurthulu, Chem. Mater. 22 (2010) 467–475.
[33] X. Wu, J. Fan, R. Ran, D. Weng, Chem. Eng. J. 109 (2005) 133–139.
[34] N.V. Skorodumova, S.I. Simak, B.I. Lundqvist, I.A. Abrikosov, B. Johansson, Phys. Rev. Lett. 89 (2002) 166601.
[35] J.H. Wang, M. Liu, M.C. Lin, Solid State Ionics 177 (2006) 939–947.
[36] R. Ran, H. Zhang, X. Wu, J. Fan, D. Weng, J. Rare Earth 32 (2014) 108–116.
[37] W.C. Chueh, A.H. McDaniel, M.E. Grass, Y. Hao, N. Jabeen, Z. Liu, S.M. Haile, K.F. McCarty, H. Bluhm, F.E. Gabaly, Chem. Mater. 24 (2012) 1876–1882.
[38] J.P.A. Neeft, F. Hoornaert, M. Makkee, J.A. Moulijn, Thermochim. Acta 287 (1996) 261–278.
[39] C. Lee, Y. Jeon, S. Hata, J. Park, R. Akiyoshi, H. Saito, Y. Teraoka, Y. Shul, H. Einaga, Appl. Catal., B 191 (2016) 157–164.
[40] K. Krishna, A. Bueno-López, M. Makkee, J. Moulijn, Appl. Catal., B 75 (2007) 189–200.
[41] M. Schmidt, A. Masson, C. Bréchignac, Phys. Rev. Lett. 91 (2003) 243401.
[42] S. Liu, X. Wu, H. Luo, D. Weng, R. Ran, J. Phys. Chem. C 119 (2015) 17218–17227.
[43] M. Haneda, A. Towataba, Catal. Today 242 (2015) 351–356.
[44] G. Corro, U. Pal, E. Ayala, E. Vidal, Catal. Today 212 (2013) 63–69.